Machine learning emulator for physics-based prediction of ionospheric response to solar wind variations

Ryuho Kataoka[1,2], Shinya Nakano[3,2,4], and Shigeru Fujita[3,4]

[1]National Institute of Polar Research, Tachikawa, 190-8518, Japan

[2]The Graduate University for Advanced Studies, SOKENDAI, Hayama, Kanagawa 240-0193 Japan

[3]The Institute of Statistical Mathematics, Tachikawa, 190-8562, Japan

[4]Center for Data Assimilation Research and Applications, Joint Support Center for Data Science Research, Tachikawa, 190-8562, Japan

Corresponding author: first and last name (kataoka.ryuho@nipr.ac.jp)

Key Points:

- Echo state network reasonably works to emulate the ionospheric outputs of global MHD simulation results.
- The ESN-based emulator suggests a missing By-assymetric density effect on the polar-cap potential.
- The ESN-based emulator is quick to run, leading to a breakthrough for space weather forecasting and data assimilation studies.

Abstract

Physics-based simulations are important for elucidating the fundamental mechanisms behind the time-varying complex ionospheric conditions, such as field-aligned currents (FACs) and plasma convection patterns, against unprecedented solar wind variations incidents in the Earth's magnetosphere. However, to perform a huge parameter survey for understanding the nonlinear solar wind density dependence of the FAC and convection patterns, for example, a large-scale cluster computer is not fast enough to run state-of-the-art global magnetohydrodynamic (MHD) simulations. Here we report the impressive performance of a machine-learning based surrogate model for the ionospheric outputs of a global MHD simulation, using the reservoir computing technique called echo state network (ESN). The trained ESN-based emulator is exceptionally fast to perform the parameter survey, suggesting a missing solar wind density dependence of the ionospheric polar cap potential. We discuss future directions including the promising application for the space weather forecast.

Plain Language Summary

We developed a machine-learning emulator to mimic a global magnetohydrodynamic (MHD) simulation of a dynamically changing auroral oval. We conducted a state-of-the-art global MHD simulation called REPPU for four magnetic storm events to experience large dynamic ranges of input solar wind parameters changes. The long-term REPPU simulation results are then used to train the machine-learning model called echo state network (ESN). Using the ESN-based emulator, we confirmed one of the well-known solar wind parameter dependences of the auroral activities on the solar wind magnetic field directions. From the parameter survey using the ESN-based emulator, we further suggest a missing nonlinear solar wind density dependence. Compared to the computationally expensive global MHD simulations, the ESN-based emulator is surprisingly quick to run, leading to a breakthrough for operational space weather forecasting and opening a pathway for future data assimilation studies of the solar wind-magnetosphere-ionosphere coupling.

1 Introduction

Machine learning (ML) techniques have been recognized as a useful tool for predicting geomagnetic activity indices, as represented by the AE, Kp, and Dst indices, using solar wind parameters as inputs, such as the solar wind speed (Vsw), proton density (Np), and interplanetary magnetic field (IMF). Many such attempts have been thoroughly reviewed by Liemohn et al. (2018). One of the latest studies used the ML technique called echo state network (ESN) to successfully predict the AE index to diagnose the nonlinearity of a magnetosphere-ionosphere coupled system using a synthetic solar wind time series (Nakano and Kataoka, 2022).

In principle, and in more detail, the high-latitude geomagnetic activity indices are products of the two-dimensional (2D) distributions of ionospheric currents, as characterized by the field-aligned currents (FACs) into and out of the ionosphere (Iijima and Potemra, 1978), ionospheric horizontal plasma flow called ionospheric convection, and height-integrated ionospheric conductivity. Detailed 2D patterns of ionospheric convection, FACs, and ionospheric conductivity can be empirically modeled as a function of the solar wind parameters and geomagnetic activity indices (Weimer, 1995; 2001; Weimer and Edwards, 2022). The empirical models, however, have limitations in that they predict the averaged observed patterns and cannot account for dynamic solar wind variations or unprecedented solar wind variations.

To overcome the limitations, a straightforward physics-based approach is to solve the idealized magnetohydrodynamic (MHD) equations for the solar wind and magnetospheric plasma flows, setting the appropriate height-integrated ionospheric conductivity layer as one of the boundary conditions. In global MHD simulations, we can obtain 2D patterns of the ionospheric convection and FACs, where auroral ovals are consistently represented by 2D patterns of the ionospheric conductivity (e.g., Tanaka et al., 2022). State-of-the-art global MHD simulations are also essential for understanding the mechanism behind the dynamically changing auroral oval distribution (e.g., Ebihara and Tanaka, 2022). Further parameter surveys using such simulations are still necessary to understand the nonlinear effects, for example, the density effect on the ionospheric potential or energy deposition (Khachikjan et al., 2008; Ebihara et al., 2019; Yang et al., 2020; Nakano and Kataoka, 2022). However, the practical use of the global MHD simulation for such a parameter-survey purpose is still limited because it is computationally expensive.

A reasonable next approach to addressing the time-comsumption issue is emulate the computationally expensive physics-based global MHD simulation by ML techniques, although the physics behind the simulation becomes a black box. Once such an ML-based emulator is developed, we can predict dynamically changing 2D maps of ionospheric conditions instantaneously. It is therefore practically possible for a small computer to make a thorough parameter survey by the ML-based emulator.

The purpose of this study is to develop such an ML-based emulator and to examine the potential impacts. While an emulation that works with a global MHD simulation was attempted for parameter tuning (Kleiber et al., 2013; Heaton et al., 2015), here we develop an ESN-based emulator for predicting the dynamic ionospheric responses of the magnetosphere-ionosphere system to variable solar-wind time-series input. The methods of emulating global MHD simulation results by the ESN model are briefly introduced in Section 2. In Section 3, we examine the obtained results from the newly developed ESN-based emulator. In Section 4, we discuss the predictive capabilities of the ESN-based emulator and some future directions.

2 Materials and Methods

2.1 Global MHD simulation

REPPU (REProduce Plasma Universe) is an MHD simulation code developed for studying the global magnetosphere-ionosphere coupling (Tanaka, 1995; Tanaka 2020). The REPPU code is characterized by an excellent ionospheric reproduction of fundamental auroral phenomena such as substorm onset (Ebihara and Tanaka, 2015a,b), sun-aligned arcs (Tanaka et al., 2017), and the theta aurora (Tanaka et al., 2018). In this study, we used an improved REPPU simulation, including the effects of a tilted dipole axis and seasonal changes of solar zenith angles. The total number of grid cells in the magnetosphere is 30722 (horizontal) times 240 (vertical), where the unstructured grid system described by Moriguchi et al. (2008) is employed. The number of grid cells in the ionosphere is 30722. The improved REPPU simulation is essentially the same as that used for the real-time REPPU simulation of space weather forecast executed by the National Institute of Information and Communications Technology (Nakamizo and Kubota, 2021). We used high-resolution OMNI-2 one-min data (Bx, By, Bz, Np, Vx, Vy, Vz, and proton temperature) for input. Note that we used B vectors in the GSM coordinate system and we provisionally used V vectors in the GSE coordinate system.

We ran a REPPU simulation to obtain several-days worth of activity outputs for training and testing the emulator. Four different long-term output datasets for moderate and intense magnetic storm events as driven by corotating interaction regions (CIR) or coronal mass ejections (CME) were connected and used for training (see Kataoka and Miyoshi (2006) for the difference between CIR and CME driven storms): Intense (Dst peak = -130 nT) CIR storm (~24 hours from 2015/10/7 0000 UT), moderate (Dst peak = -56 nT) CIR strm (~21 hours from 2015/10/18 0000 UT), moderate (Dst peak = -87 nT) CME storm (~34 hours from 2015/11/06 1200 UT), and intense (Dst peak at -166 nT) CME storm (~36 hours from 2015/12/19 1200 UT). Further, we prepared the testing data from non-storm time 16.5-hour data from 2015/09/06 0000 UT. Note also that we discarded the first one hour of data for each run, in which the global plasma distribution cannot yet be physically realistic.

We used 10-min averaged output data for the ionospheric potential Φ, FAC J//, and height-integrated conductivity maps. The ionospheric potential contours represent the ionospheric convection pattern. The FAC is positive for upward (out of the ionosphere) and negative for downward (into the atmosphere). The selected height integrated conductivity Σxx is a tensor component, where x is positive to the north and y is positive to the east. For coarse-graining purposes, as well as to clearly resolve the Region-1 and Region-2 FAC patterns, we binned the Φ, J//, and Σxx maps for the northern polar region (>50 deg latitude) into 15 × 32 in latitude and longitude, respectively, from the original resolution of 60 × 320.

We then applied principal component analysis (PCA) to the 2D maps of the simulation results to reduce the dimensions. Note that Cousins et al. (2015) applied a similar method to evaluate variable FAC patterns. In this study we used the PCA module of Python 3 scikit-learn (https://scikit-learn.org/stable/modules/generated/sklearn.decomposition.PCA.html). To reproduce the > 90% variance of the original features, we decomposed the J// pattern into 15 PCA components, and the Φ and Σxx patterns into 10 PCA components (Supplemental Information Figures S1 and S2).

2.2 Machine learning technique

We require an ML technique that can be trained by a small training dataset because the REPPU simulation is still computationally expensive for long runs. Therefore, the standard deep learning technique is not appropriate. We also need a specific ML technique suitable for time-series prediction, because the ionosphere dynamically changes following the time history in the magnetosphere and ionosphere. Both needs can be satisfied by the reservoir computing method ESN (Jaeger, 2001; Jaeger and Haas, 2004), as reviewed by Tanaka et al. (2019). We used essentially the same ESN method as documented by Kataoka and Nakano (2021) and Kataoka et al. (2022). In this study we used the ESN module of Python 3 as developed by Tanaka et al. (2022) (See https://github.com/GTANAKA-LAB/DTS-ESN/).

The basic ESN model used in this study is described by the reservoir sate vector **x** and the model output vector **y** (time series of PCA components of J//, Σxx, and Φ) at $t = n + 1$ steps as follows:

$$\mathbf{x}(n+1) = \tanh\left\{W^{in}\mathbf{u}(n+1) + W\mathbf{x}(n)\right\}, \tag{1}$$

$$\mathbf{y}(n+1) = W^{out}\mathbf{x}(n+1)\,. \tag{2}$$

Here, the weight matrices W^{in} and W are multiplied by the input vector **u** (the solar wind time series) and the reservoir state vector **x**, respectively. In this study, we set the number of the nodes (elements of **x**) to be 300. These W^{in} and W are fixed, while only W^{out} is trained by the Ridge regularization with regularization parameter of 10^{-3}.

To create the random and sparse node connections of W, where only 10% of the matrix elements are random values between -1.0 and 1.0, and the remaining 90% are zero. We chose the optimal spectral radius (maximum eigenvalue of *W*) to be 0.55, 0.60, and 0.65 for J//, Σxx, and Φ, respectively, by evaluating the normalized root-mean square errors using both training and testing data (Supplemental Information Figure S3). As the input vectors **u**, the solar wind speed and density are roughly normalized as $\log_{10}$ Vsw - 2.5, and $\log_{10}$ Np - 1.0 before training the ESN model. It is noteworthy here that both the speed and density follow log-normal distributions (Burlaga and Lazarus, 2000).

We constructed the emulators for J//, Σxx, and Φ maps, independently. However, the current continuity J// = div(Σ grad Φ) relates these three parameters and any inconsistencies among the three parameters therefore give hints of unphysical parts of the emulator to potentially fix, or avenues to evaluate errors in the emulation results for future applications.

3 Results and discussions

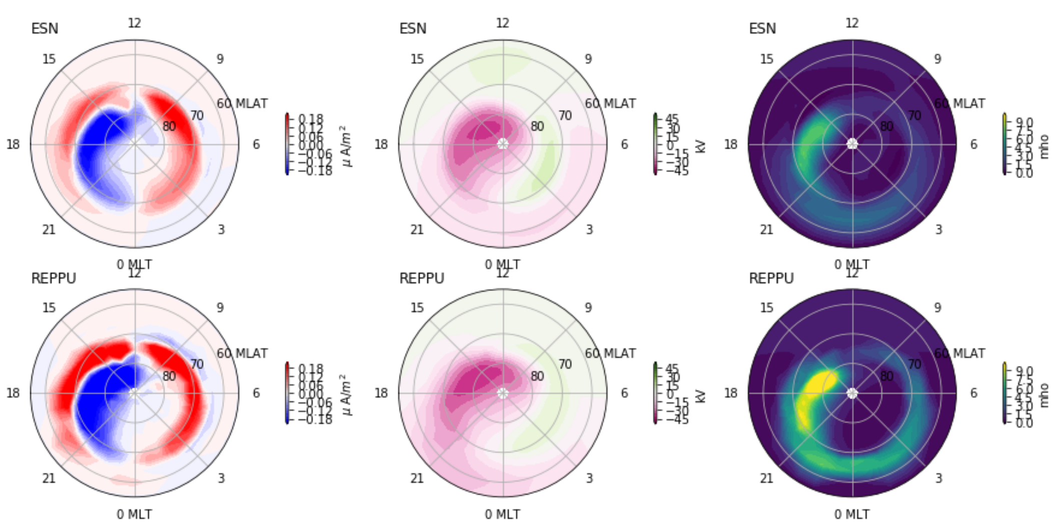

Figure 1. Snapshot example of field-aligned currents, ionospheric potential, and conductivity maps obtained from ESN emulator (top) and REPPU simulation (bottom) at a testing time of t = 735 steps.

An example result from the ESN-based emulator compared with a REPPU simulation is shown in Figure 1. We can see a reasonable agreement between the results from ESN-based emulator and REPPU simulation; such as Region 1 and Region 2 FAC patterns and two-cell convection patterns, although the strong conductivity enhancement in the dusk sector was not reproduced. See Supplemental Information Movie S1-S3 for the other time intervals.

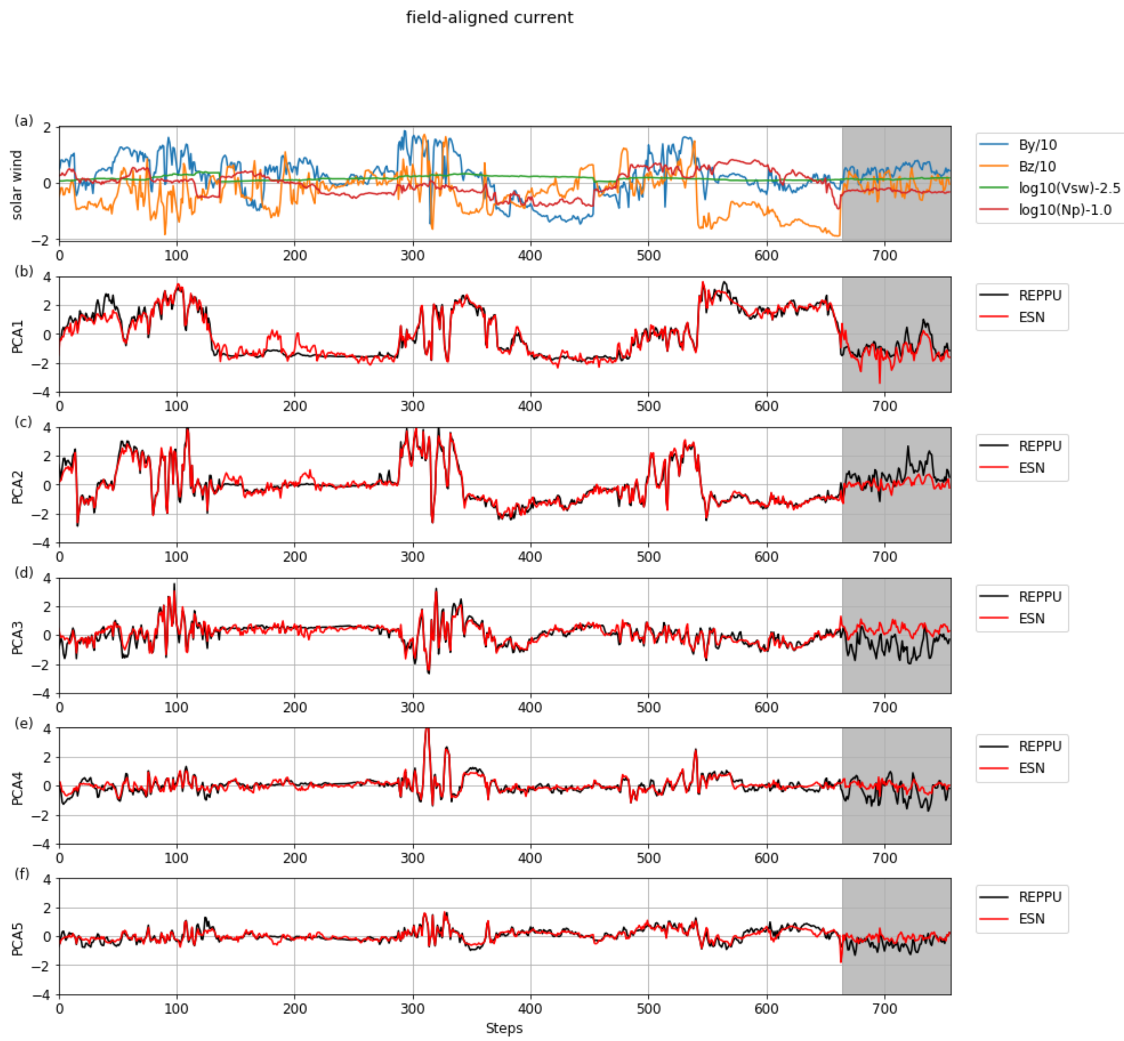

Figure 2. Solar wind parameters (a) and top five PCA components (b-f) for FAC. Black curves show the REPPU simulation results and the red curves are from the ESN model. The testing time interval, which are not used for training but used for score evaluation, is shown by the gray hatched time interval.

Figure 2 shows the performance of training and testing the ESN emulator of the FAC map. See Supplemental Information Figures S4-S5 for the same figures for potential and conductivity. The input solar wind parameters are shown in the top panel. The top five PCA components and the prediction from the ESN model are shown. The training interval is t < 664 steps. The trained ESN model reproduces the time variation of PCA components for both the training and the testing intervals.

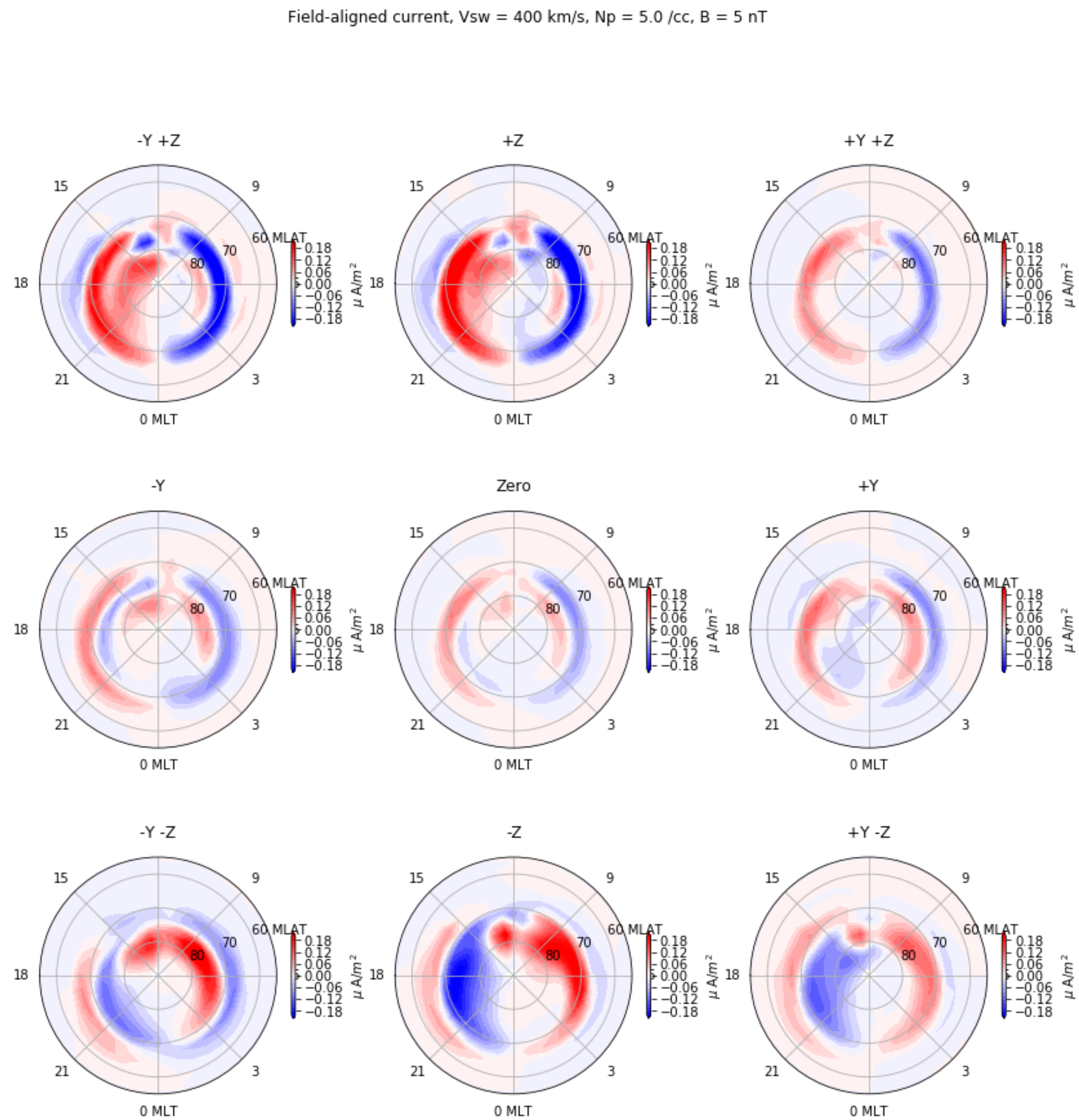

Figure 3. Quasi-steady state FAC patterns as obtained from the ESN-based emulator for different IMF clock angles using synthetic solar wind data.

Instead of directly comparing the emukation results with the observation data, which are available only for spatially limited areas, we benchmark the emulation results against the standard empirical models (Weimer, 1995; 2001). Figures 3 and 4 show an example of the IMF clock-angle dependence of FAC and convection patterns using synthetic solar wind data (Supplemental Information Figure S6), fixing the density at Np = 5 /cc, the solar wind speed at Vsw = 400 km/s, and the IMF strength at B0 = 5 nT. We selected the results from quasi-steady state time steps for each IMF directions (i.e., 15 steps = 150 min after the IMF changes). The IMF By and Bz dependence of the Region-1 and Region-2 FAC system as well as the overall convection pattern morphology show a reasonable agreement with those as they appears in the Weimer models (Weimer, 1995; 2001); such as pairs of Region 1 and Region 2 FAC patterns

(Figure 3) with round-cell and clecent-cell convection patterns (Figure 4) and their IMF By dependence during southward IMF Bz (SBZ) conditions.

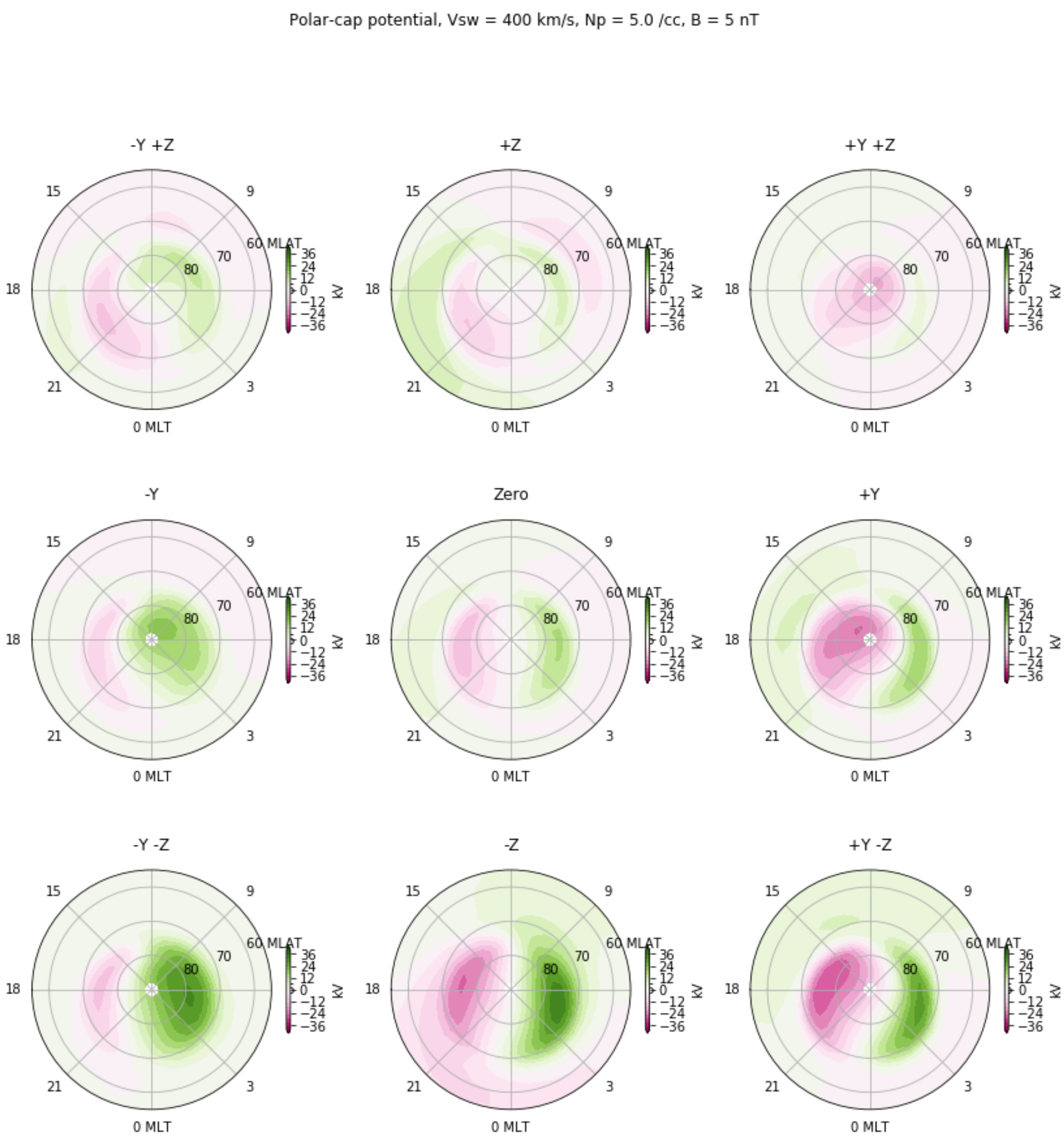

Figure 4. Quasi-steady state ionospheric potential map as obtained from the ESN-based emulator for different IMF clock angles using synthetic solar wind data.

For comparison with empirical models, there is a notable drawback of this study by selecting active-time magnetic storm events as the training data set. Note that the unrealistically large-amplitude of the Region-2 FAC appeared during the northward IMF (NBZ) due to a poor sample of the NBZ situation in the training data. Further dataset which includes plenty enought NBZ situation are therefore needed to correctly train the emulator model for NBZ conditions.

Note that the ESN-based emulator can even learn from the other global MHD simulation results if necessary, and the ring current coupled MHD simulation (e.g. Kataoka et al., 2005) would also be interesting to be included for further discussing the dynamic evolution of Region-2 FAC system in future.

The ESN-based emulator is exceptionally fast to run and it is useful for a thorough parameter survey of so-called heatmap analysis, which cannot be done by observations or simulations. As an example, we input the synthetic solar wind variations to the ESN-based emulator to examine the nonlinear density effect on the cross-polar cap potential (CPCP), as shown in Supplemental Information Figures S7-S8. Note that it is computationally expensive for the REPPU simulation to obtain the following heatmap results. Note also that we fixed the solar wind speed in the input, so that the density effect is essentially the same as the dynamic pressure effect.

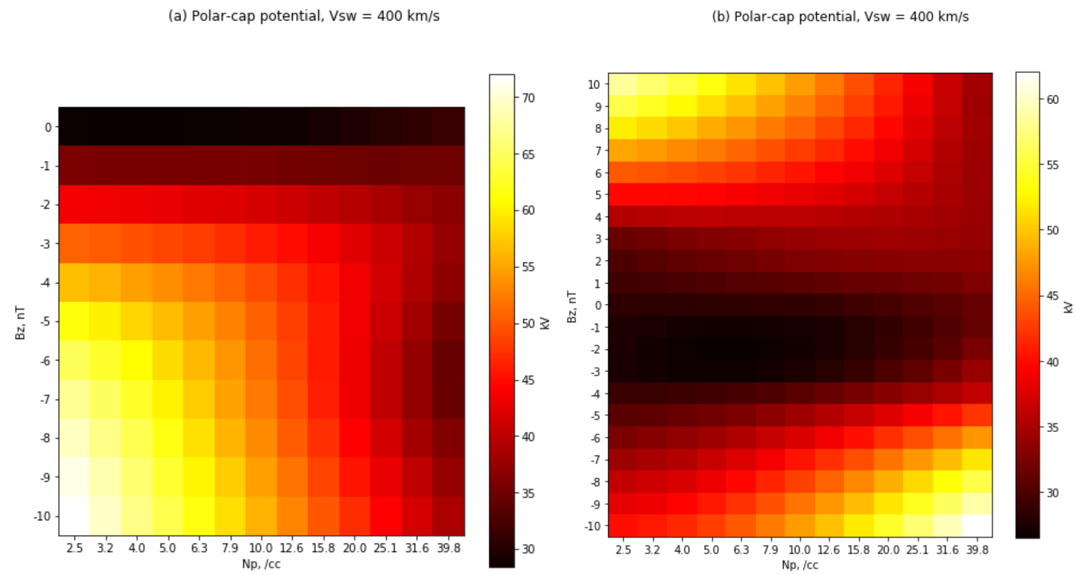

Figure 5. Heatmap analysis of the parameter survey to examine the nonlinear density effect on the cross polar-cap potential, changing (a) SBZ and (b) By component using the ESN-based emulator.

As shown in Figure 5a, the CPCP has a negative dependence on the density during strong SBZ. In fact, the similar tendency has been identified by Khachikjan et al. (2008) using active-time SuperDARN observations. Khachikjan et al. (2008) discussed that the shrinking dayside magnetopause by high dynamic pressure may be relevant to reduce the possible effect of dayside reconnection that is powering the CPCP.

Recognizing that the overall IMF By dependence was fairly reproduced by the ESN-emulator as shown in Figures 3 and 4, we further diagnose the density dependence by changing the IMF By component, turning off the contribution of SBZ. From the heatmap analysis without SBZ component, Figure 5b shows that the density dependence is positive when By < 4 nT, while it is negative for larger By. The By-aymmetric density effect is a new problem “predicted” from the ESN-based emulator, which suggests that the nonlinear density effect on CPCP can be more complex than imagined from the SBZ reconnection hypothesis. Note that the IMF By dependence does not clearly appear if we integrate the obtaind By-Np heatmap in density, which is consistent with SuperDARN observations (Mori and Kustov, 2013). Related future works therefore include the observation-based identification of the By-aymmetric density effect as well as the detailed analysis of the global MHD simulation results of both magnetosphere and ionosphere to identify of the exact mechanism to cause the By-aymmetric density effect.

In this study we used simulation data for CIR- and CME-driven magnetic storm events that occurred in the fall to winter seasons. The training data set is therefore limited to the particular situation where the auroral activity is high and the northern hemisphere is darker than the southern hemisphere. A detailed discussion of the sunlight effect associated with solar zenith angles and the general north-south asymmetry are therefore interesting future subjects of study when we have accumulated more long-term REPPU simulation results, including different seasons.

More generally, the ESN-based emulator is capable of dynamic predictions following the time history, and this study investigated the performance of reconstructing the 10-min scale dynamics. In such a time scale, the ESN-based model developed in this study can be readily applicable to the operational space weather forecast by replacing the input file by the real-time solar wind data. Emulating more dynamic phenomena such as sudden commencements and substorms is therefore the next technical challenge. The ESN method can be applied to diverse temporal scales (Tanaka et al., 2022), and in future studies we plan to tune the ESN-based emulator to a higher time resolution, choosing the right leaking rate matrix to reproduce both min-scale to 10-min scale dynamics.

This paper presented the first kick-off results to demonstrate the potential impact of the emulator. For a practical use, the accuracy must be improved by learning NBZ and other variable conditions. Future studies using the ESN emulator of the REPPU simulation therefore include an examination of the accuracy in reproducing observation data, such as SuperDARN convection maps. Any partial data or point data can also be used with cutting-edge data assimilation techniques (Nakano et al., 2020). For data assimilation, we need to increase the ensemble number of simulation runs for integrating large probabilistic ensembles, and the ESN-based emulator will play an essential role. In this manner, the ESN-based emulator can be expected to become a basic technique for future space weather reanalysis studies.

4 Conclusions

Using the ESN model trained by long-term REPPU simulation runs for magnetic storm events, we developed an emulator to instantaneously reproduce the REPPU simulation results for the ionospheric conditions by inputting the solar wind parameter time series. The newly developed ESN-based emulator reasonably reproduces the active-time 2D patterns of the ionospheric potential, FAC, and conductivity. A missing By-assymetric density effect is also suggested from the parameter survey using the ESN-based emulator. The ESN-based emulator can lead to breakthrough advances for real-time space weather forecasting operations as well as for accelerating the data assimilation studies.

Acknowledgments

We acknowledge the use of NASA high-resolution OMNI data (https://omniweb.gsfc.nasa.gov/ow_min.html). The REPPU simulation was performed with the computing facilities at the Center for Engineering and Technical Support of the Institute of Mathematical Statistics and the Polar Science Computer System at the National Institute of Polar Research (NIPR). This research was supported by "Challenging Exploratory Research Projects for the Future" grant from the Research Organization of Information and Systems (ROIS). This study is part of the Science Program of Japanese Antarctic Research Expedition (JARE) Prioritized Research Project AJ1007 (Space environmental changes and atmospheric response explored from the polar cap), supported by NIPR under MEXT.

Open Research

The python codes and the training dataset for the ESN-based emulator model used in this study is open to public at https://github.com/ryuhokataoka/REPPU-ESN (v1.0.0 is released at doi.org/10.5281/zenodo.7519025)

References

Burlaga, L. F., & Lazarus, A. J. (2000). Lognormal distributions and spectra of solar wind plasma fluctuations: Wind 1995-1998. Journal of Geophysical Research, 105(A2), 2357-2364. https://doi.org/10.1029/1999JA900442

Cousins, E. D. P., T. Matsuo, A. D. Richmond, and B. J. Anderson (2015), Dominant modes of variability in large-scale Birkeland currents, J. Geophys. Res. Atmos., 120, 6722-6735, doi:10.1002/2014JA020462.

Ebihara, Y., and T. Tanaka (2015a). Substorm simulation: Formation of westward traveling surge. Journal of Geophysical Research: Space Physics, 120(12), 10466–10484. https://doi.org/10.1002/2015JA021697

Ebihara, Y., and T. Tanaka (2015b). Substorm simulation: Insight into the mechanisms of initial brightening. Journal of Geophysical Research: Space Physics, 120(9), 7270–7288. https://doi.org/10.1002/2015JA021516

Ebihara, Y., Tanaka, T., & Kamiyoshikawa, N. (2019). New diagnosis for energy flow from solar wind to ionosphere during substorm: Global MHD simulation. Journal of Geophysical Research: Space Physics, 124, 360-378. https://doi.org/10.1029/2018JA026177

Ebihara, Y., and T. Tanaka (2022). Where is Region 1 field-aligned current generated? Journal of Geophysical Research: Space Physics, 127, e2021JA029991. https://doi.org/10.1029/2021JA029991.

Heaton, M. J., W. Kleiber, S. R. Sain, and M. Wiltberger (2015). Emulating and calibrating the multiple-fidelity Lyon-Feddder-Mobarry magnetosphere-ionosphere coupled computer model. Journal of the Royal Statistical Society. Series C (Applied Statistics), 64(1), 93-113. http://www.jstor.org/stable/24771865

Iijima, T., and T. A. Potemra (1978), Large-scale characteristics of field-aligned currents associated with substorms, J. Geophys. Res., 83(A2), 599-615, doi:10.1029/JA083iA02p00599.

Jaeger, H. (2001). The "echo state" approach to analysing and training recurrent neural networks GMD Report 148. GMD – German National Research Institute for Computer Science.

Jaeger, H. and H. Haas (2004) Harnessing nonlinearity: Predicting chaotic systems and saving energy in wireless communication, Science, 304, 78–80, https://doi.org/10.1126/science.1091277.

Kataoka, R., D. H. Fairfield, D. G. Sibeck, L. Rastaetter, M.-C. Fok, T. Nagatsuma, and Y. Ebihara (2005), Magnetosheath variations during the storm main phase on 20 November 2003: Evidence for solar wind density control of energy transfer to the magnetosphere, Geophys. Res. Lett., 32, L21108, doi:10.1029/2005GL024495.

Kataoka, R., and Y. Miyoshi (2006), Flux enhancement of radiation belt electrons during geomagnetic storms driven by coronal mass ejections and corotating interaction regions, Space Weather, 4, S09004, doi:10.1029/2005SW000211.

Kataoka, R., and S. Nakano (2021), Reconstructing solar wind profiles associated with extreme magnetic storms: A machine learning approach, Geophysical Research Letters, 48, e2021GL096275. https://doi.org/10.1029/2021GL096275.

Kataoka, R., T. Sato, C. Kato, A. Kadokura, M. Kozai, S. Miyake, K. Murase, L. Yoshida, Y. Tomikawa, and K. Munakata (2022), Local environmental effects on cosmic ray observations at Syowa Station in the Antarctic: PARMA-based snow cover correction for neutrons and machine learning approach for neutrons and muons, J. Space Weather Space Clim., Volume 12, 37, https://doi.org/10.1051/swsc/2022033

Khachikjan, G. Y., A. V. Koustov, and G. J. Sofko (2008), Dependence of SuperDARN cross polar cap potential upon the solar wind electric field and magnetopause subsolar distance, J. Geophys. Res., 113, A09214, doi:10.1029/2008JA013107.

Kleiber, W., S. R. Sain, M. J. Heaton, M. Wiltberger, C. S. Reese and D. Bingham (2013), PARAMETER TUNING FOR A MULTI-FIDELITY DYNAMICAL MODEL OF THE MAGNETOSPHERE, The Annals of Applied Statistics, Vol. 7, No. 3, 1286-1310.

Liemohn, M. W., McCollough, J. P., Jordanova, V. K., Ngwira, C. M., Morley, S. K., Cid, C., et al. (2018). Model evaluation guidelines for geomagnetic index predictions. Space Weather, 16, 2079-2102. https://doi.org/10.1029/2018SW002067

Mori, D., and A. V. Kustov (2013), SuperDARN cross polar cap potential dependence on the solar wind conditions and comparisons with models, Adv. Space Res., 52, 1155-1167, http://dx.doi.org/10.1016/j.asr.2013.06.019

Moriguchi, T., A. Nakamizo, T. Tanaka, T. Obara, and H. Shimazu (2008). Current systems in the Jovian magnetosphere, J. Geophys. Res., 113, A05204, doi:10.1029/2007JA012751.

Nakamizo A., and Y. Kubota (2021), Research and Development of Global Magnetosphere MHD Simulation, NICT Research Report, Vol. 67, No. 1 (in Japanese with English abstract), https://www.nict.go.jp/data/research-report/index.html

Nakano, S., T. Hori, K. Seki, et al. (2020), A framework for estimating spherical vector fields using localized basis functions and its application to SuperDARN data processing. Earth Planets Space 72, 46. https://doi.org/10.1186/s40623-020-01168-4

Nakano, S. and R. Kataoka (2022), Echo state network model for analyzing solar-wind effects on the AU and AL indices, Ann. Geophys., 40, 11-22, https://doi.org/10.5194/angeo-40-11-2022.

Tanaka, G., Yamane, T., Heroux, J. B., Nakane, R., Kanazawa, N., Takeda, S., et al. (2019). Recent advances in physical reservoir computing: A review. Neural Networks, 115, 100-123. https://doi.org/10.1016/j.neunet.2019.03.005

Tanaka, G., T. Matsumori, H. Yoshida, and K. Aihara (2022), Reservoir computing with diverse timescales for prediction of multiscale dynamics, Phys. Rev. Research 4, L032014, doi:10.1103/PhysRevResearch.4.L032014

Tanaka, T., Obara, T., Watanabe, M., Fujita, S., Ebihara, Y., & Kataoka, R. (2017). Formation of the Sun-aligned arc region and the void (polar slot) under the null-separator structure. Journal of Geophysical Research: Space Physics, 122(4), 4102–4116. https://doi.org/10.1002/2016JA023584

Tanaka, T., Obara, T., Watanabe, M., Fujita, S., Ebihara, Y., Kataoka, R., & Den, M. (2018). Cooperatives roles of dynamics and topology in generating the magnetosphere-ionosphere disturbances: Case of the theta aurora. Journal of Geophysical Research: Space Physics, 123(12), 9991–10008. https://doi.org/10.1029/2018JA025514

Tanaka, T., Watanabe, M., Ebihara, Y., Fujita, S., Nishitani, N., & Kataoka, R. (2022). Unified theory of the arc auroras: Formation mechanism of the arc auroras conforming general principles of convection and FAC generation. Journal of Geophysical Research: Space Physics, 127, e2022JA030403.

Weimer, D. R. (1995), Models of high-latitude electric potentials derived with a least error fit of spherical harmonic coefficients, J. Geophys. Res., 100(A10), 19595-19607, doi:10.1029/95JA01755.

Weimer, D. R. (2001), Maps of ionospheric field-aligned currents as a function of the interplanetary magnetic field derived from Dynamics Explorer 2 data, J. Geophys. Res., 106(A7), 12889-12902, doi:10.1029/2000JA000295.

Weimer, D. and T. Edwards (2021), Testing the electrodynamic method to derive height-integrated ionospheric conductances, Ann. Geophys., 39, 31-51, https://doi.org/10.5194/angeo-39-31-2021

Yang, Z., Zhang, B., Lei, J., and Dang, T. (2020). Nonlinear response of the cross polar cap potential to solar wind density under northward interplanetary magnetic field. Geophysical Research Letters, 47, e2020GL087559. https://doi.org/10.1029/2020GL087559